Fractional diffusion theory of balanced heterogeneous neural networks

Asem Wardak ⬤ and Pulin Gong ⬤*

School of Physics, University of Sydney, New South Wales 2006, Australia

Interactions of large numbers of spiking neurons give rise to complex neural dynamics with fluctuations occurring at multiple scales. Understanding the dynamical mechanisms underlying such complex neural dynamics is a long-standing topic of interest in neuroscience, statistical physics and nonlinear dynamics. Conventionally, fluctuating neural dynamics are formulated as balanced, uncorrelated excitatory and inhibitory inputs with Gaussian properties. Yet heterogeneous, non-Gaussian properties have been widely observed in both neural connections and neural dynamics. Based on balanced neural networks with heterogeneous, non-Gaussian features, our analysis reveals that synaptic inputs possess power-law fluctuations in the limit of large network size, leading to a remarkable relation between complex neural dynamics and the fractional diffusion formalisms of nonequilibrium physical systems. We derive a fractional Fokker-Planck equation with analytically tractable boundary conditions for the network, uniquely accounting for the leapovers caused by the fluctuations of spiking activity. This body of formalisms represents a fractional diffusion theory of heterogeneous neural networks and results in an exact description of the network activity states. In particular, the fractional diffusion theory identifies a dynamical state at which the neural response is maximized as a function of structural connectivity. This state is then implemented in a balanced spiking neural network and displays rich, nonlinear response properties, providing a unified account of a variety of experimental findings on neural dynamics at the individual neuron and network levels, including fluctuations of membrane potentials and population firing rates. Our theory and its network implementations provide a framework for investigating complex neural dynamics emerging from large networks of spiking neurons and their functional roles in neural processing.

I. INTRODUCTION

Networks composed of a large number of interacting units are ubiquitous in physical, biological, financial, and ecological systems [1–4]. In these systems, interactions of units give rise to complex network dynamics with great fluctuations occurring at multiple spatial and temporal scales [1–4]. Understanding such complex dynamics is a long-standing topic of common interest in these diverse systems. In neuroscience, neural networks of many interacting neurons likewise exhibit great fluctuations in their firing activity [5–7]; such fluctuations provide a critical window into understanding the working mechanism of neural systems. The classical theoretical framework for understanding how complex neural dynamics emerge is based on homogeneous, randomly coupled networks with balanced excitation and inhibition [8–12]. Such balanced network models have successfully reproduced many experimental observations such as the high irregularity of neural firing activity and broad distributions of firing rates, and have been analyzed using dynamical mean field models with the assumption of homogeneous Gaussian noise

as synaptic inputs, often referred to as the normal diffusion theory [8–10]. The standard Fokker-Planck formalism is then used in this theoretical framework to obtain the key statistical properties of complex neural dynamics. Virtually all existing balanced neural network models, including the classical ones [8–10] and their recent extensions incorporating heterogeneous degrees [13–15], distance-dependent connectivity [16–18], and alternative neuron models such as conductance-based neurons [19,20], have been studied by applying such normal-diffusion-based formalisms.

Recent experimental studies, however, have been increasingly demonstrating that heterogeneous, non-Gaussian properties are ubiquitous for both neural connectivity and neural activity dynamics. For instance, it has been found that synaptic connection strengths [21,22] and the number of synaptic connections [23] exhibit heavy-tailed distributions with non-Gaussian features. Furthermore, it has been empirically found that neural firing activity has super-Poisson dynamics [7], with great heterogeneity and fluctuations occurring at multiple scales [24–26], and that membrane potentials fluctuate far from the firing threshold [27]. Some of these properties are not necessarily incompatible with Gaussian input statistics: non-Gaussian, lognormal distributions of synaptic strengths lead to the classical, normal diffusion theory in the large network limit. Suitable assumptions on the classical theory such as adaptation can be incorporated into individual modeling studies, in order to reproduce individual phenomena such as large fluctuations of membrane potentials [28]. Nevertheless, the fundamental problems of whether

---

*pulin.gong@sydney.edu.au

and how the non-Gaussian features of neural dynamics can be explained in a unified theoretical framework, and the mechanistic relationships between these neural dynamics and heterogeneous connectivity, remain unclear.

Here, extending the classical theory of balanced networks, we develop a theory explaining how the non-Gaussian features of complex neural dynamics emerge from biologically realistic, heterogeneous neural networks. Based on balanced spiking neural networks with heterogeneous connection strengths, our analysis reveals that synaptic inputs in such heterogeneous networks possess heavy-tailed, Lévy fluctuations, a type of fluctuation typical for nonequilibrium systems with many interacting units [29–31]. This thus leads to a relation between complex neural dynamics and fractional diffusion formalisms developed for studying nonequilibrium physical systems [32–37]; correspondingly, we refer to this as the fractional diffusion theory of balanced neural networks. In our fractional theory, we mathematically demonstrate how these biologically realistic neural networks lead to membrane potentials undergoing fractional, Lévy diffusion instead of the normal, Brownian diffusion arising in homogeneous networks. By uniquely accounting for the Lévy leapovers caused by the great fluctuations of spiking activity, we develop an analytically tractable fractional Fokker-Planck equation with absorbing boundary conditions. The fractional theory leads to an exact description of the activity states of balanced heterogeneous neural networks; we verify our theory in spiking neural network models. We also demonstrate how heterogeneous firing rate distributions can be analytically incorporated into our fractional diffusion theory.

Based on this fractional diffusion theory of heterogeneous neural networks, we identify a network state which is fundamentally different from the asynchronous irregular state and the synchronous irregular state in the conventional models [9,10,38]. Due to the fractional nature of this state, we term it the fractional state. This state exhibits rich nonlinear response properties and can explain a variety of complex neural dynamics at the individual-neuron and circuit levels, which otherwise would be treated in isolation in previous studies. In this state, membrane potential resides far from the threshold, exhibiting heavy-tailed, skewed distributions, quantitatively consistent with neurophysiological recordings in the visual cortex of awake monkeys [27]. Neural firing activity exhibits great variability with firing rate fluctuations, as observed in Refs. [7,24,26]. The collective firing rate fluctuations of neural networks happen at multiple scales in a scale-free manner, as widely observed in experimental studies [25,39]. We further demonstrate that in this fractional state, the neural response is maximized as a function of structural connectivity, indicating that the heterogeneity of neural connectivity has an impact on neural dynamics. Our fractional diffusion framework not only provides a unified account of a variety of the key features of neural dynamics, but can also be applied to understand how complex dynamics emerge from other nonequilibrium systems with large numbers of interacting units.

II. HETEROGENEOUS NETWORK MODEL

We consider a generalization of the classical homogeneous networks which have been extensively studied over the past two decades [8–11,38,40]. Our circuit model consists of N_E excitatory and N_I inhibitory neurons. Each neuron receives C_E and C_I connections from excitatory and inhibitory neurons, respectively, and C_{ext} from excitatory neurons outside the network. The membrane potential $V_i(t)$ of neuron $i \in \{1, \ldots, N_E + N_I\}$ satisfies the equation for a leaky integrate-and-fire neuron [10],

$$\tau \dot{V}_i(t) = -V_i(t) + I_i(t), \qquad (1)$$

where τ is the integration time, and $I_i(t)$ denotes the total synaptic current to neuron i. The current is modeled as a weighted sum of δ functions representing spikes from incoming neurons,

$$I_i(t) := \tau \sum_{j=1}^{C_E + C_I + C_{\text{ext}}} J_{ij} \sum_k \delta\big(t - t_j^k - D\big), \qquad (2)$$

where J_{ij} is the synaptic connection strength from neuron j to neuron i; t_j^k is the emission time of the kth spike of neuron j; and D is the transmission delay. The spikes of external neurons are modeled as independent excitatory neurons with Poisson spike trains at rate ν_{ext}. The ith neuron spikes when $V_i(t)$ reaches the firing threshold θ, resetting the membrane potential to the reset potential V_r after a refractory period τ_{rp} during which the membrane potential is unresponsive to input.

In previous studies, heterogeneous heavy-tailed distributions of synaptic weights have been fitted to lognormal distributions [21–23]. Because of the central limit theorem, in the thermodynamic limit of large network size, the dynamics of neural networks with lognormal coupling weights should be equivalent to those under the homogeneous Gaussian hypothesis [Fig. 1(a)], yielding the classical asynchronous state with Poisson-like spikes. To theoretically explore the effect of heterogeneous connectivity on network dynamics, we assume that the heavy-tailed distributions of synaptic weights are power laws, the same assumption made in Ref. [41] to theoretically study the effect of heterogeneous connectivity on neural dynamics. Recent experimental studies have found the existence of power-law synaptic strengths in drosophila whole brain data [42,43], but note that these are not mammalian brain data. In our heterogeneous network model [Fig. 1(b)], heavy-tailed distributions of outgoing synaptic weights J_{ij} are approximated by power law distributions. This power-law assumption, as demonstrated in the following sections, leads to a fractional diffusion framework that accounts for a variety of non-Gaussian properties of neural dynamics such as the infrequent large fluctuations of membrane potential and the power-law scaling of the Fano factor of spike counts. The relationship between the outgoing, statistically independent synaptic strengths in the excitatory (J_E) and inhibitory (J_I) populations is $\langle J_I \rangle = g \langle J_E \rangle = gJ$, where g is a balance factor describing the relative strength of inhibitory inputs, and $J := \langle J_E \rangle = \langle J_{\text{ext}} \rangle$.

A. Fractional diffusion formalism for heterogeneous networks

As in the classical normal diffusion theory for homogeneous networks [8–11,13–20], we consider the dynamics of our heterogeneous network in the limit of large network size. By using the generalized central limit theorem [44], we
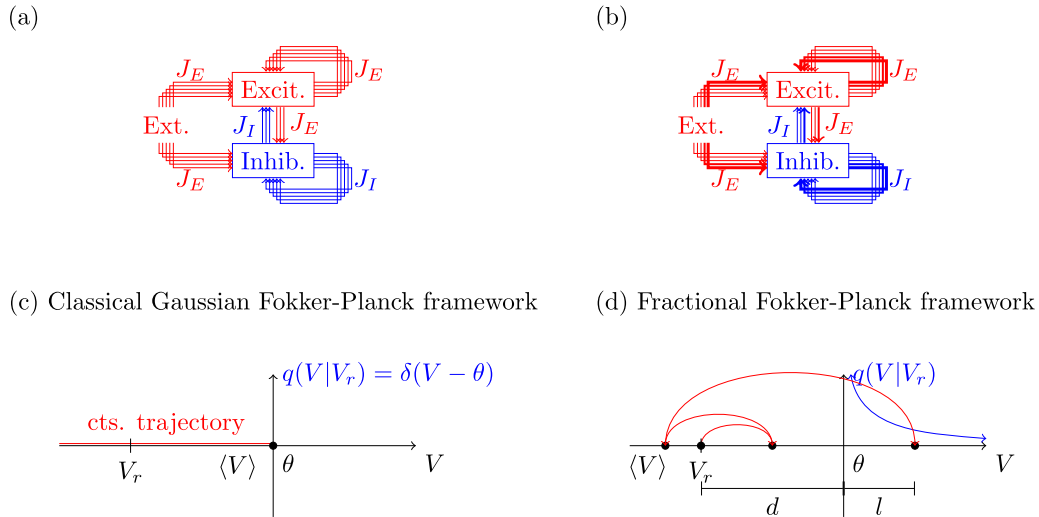
FIG. 1. Schematic of the stochastic formalisms of homogeneous and heterogeneous networks. (a) The classical formalism begins with a network model where the connection strengths J_{ij} are constant (or drawn from a Gaussian distribution), denoted by the lines of J_E and J_I with constant thickness. The classical theory leads to a Fokker-Planck framework (c), where the membrane potential V resides close to the threshold θ with Gaussian fluctuations; it thus never crosses the threshold without passing through it (first arrival equaling first passage) and so the sink is a delta function at the threshold. (b) The network is strongly heterogeneous and the connection strengths are drawn from a power-law distribution, denoted by the lines with different thicknesses, leading to a fractional Fokker-Planck formalism (d) whereby the membrane potential resides far from the threshold and has occasional large fluctuations, due to the presence of large jumps in the trajectory. This leads to leapovers l over the boundary which must be accounted for correctly in the fractional Fokker-Planck equation by using the first passage leapover density as a spatially extended sink.

rigorously prove that the total synaptic input $I(t)$ to an individual neuron in the network has nonequilibrium Lévy fluctuations, in the limit of large network size, if and only if the distributions J_r of synaptic strengths outgoing from population $r \in \{E, I, \text{ext}\}$ have a power-law tail (see detailed derivation in Appendix A). For all other distributions with well-defined asymptotic tails, however, the classical Gaussian fluctuations are recovered.

The total synaptic current $I(t)$ to a given network neuron is thus expressed as the sum of an average term with a fluctuating Lévy noise term,

$$I(t) = \mu(t) + \sigma(t)\tau^{1-1/\alpha}\eta(t). \qquad (3)$$

The noise term $\eta(t)$ is driven by an α-stable Lévy process $L = L(\alpha, \beta, \gamma_L, D_L)$ [45] with Lévy stable index $1 < \alpha \leqslant 2$, skew parameter β given by Eq. (A23),

$$\beta = \frac{(1 - \gamma g^\alpha)\nu(t - D) + \nu_{\text{ext}}}{(1 + \gamma g^\alpha)\nu(t - D) + \nu_{\text{ext}}}, \qquad (4)$$

center $\gamma_L = 0$, and scale D_L determined by the tails of the connection strength distributions J_r. The classical diffusive case is recovered when $\alpha = 2$, at which point the Lévy process $L(2, \beta, 0, D_L) = \mathcal{N}(0, 2D_L)$ reduces to a Gaussian process. The term $\nu(t)$ represents the mean population firing rate at time t. The mean input term $\mu(t)$ is a sum of internal and external inputs to the neuron, while $\sigma(t)$ is the fluctuation in the sum of the internal and external inputs (see Appendix A),

$$\mu(t) := J\tau C[\nu(t - D)(1 - \gamma g) + \nu_{\text{ext}}], \qquad (5)$$

$$\sigma(t) := J[\tau C(\nu(t - D)(1 + \gamma g^\alpha) + \nu_{\text{ext}})]^{1/\alpha}. \qquad (6)$$

Here, for clarity, we have taken $N_I = \gamma N_E$, $C := C_E = C_{\text{ext}}$, and $C_I = \gamma C$, where $\gamma = 0.25$ is the ratio of inhibitory to excitatory neurons; the general equation without these constraints is given by Eq. (A21). As in previous studies on the classical normal diffusion theory [13,14], this formalism can be extended to compute population firing rate distributions $\nu_r(t)$; a mean-field method for this under the fractional formalism is detailed in Appendix B.

Using the relation $dL = \eta(t)dt$, the dynamics of the neurons in Eq. (3) can be expressed using a Langevin-style stochastic differential equation,

$$dV(t) = \frac{-V(t) + \mu(t)}{\tau} dt + \frac{\sigma(t)}{\tau^{1/\alpha}} dL. \qquad (7)$$

The membrane potential can thus be regarded as a particle driven by Lévy noise, moving in a quadratic external well centered at $\mu(t)$.

The external input ν_{ext} is expressed in units of $\nu_{\text{thr}} = \theta/(CJ\tau)$, which is the external frequency required for the mean input $\mu(t)$ to reach threshold in the absence of recurrent feedback. When the populations are balanced ($g = \gamma^{-1} = 4$), we obtain the balance condition in the sense of Ref. [15],

$$\mu(t) = J\tau C[\nu(t - D)(1 - \gamma g) + \nu_{\text{ext}}] \approx \theta, \qquad (8)$$

which is satisfied for $(g, \nu_{\text{ext}}) = (\gamma^{-1}, \nu_{\text{thr}})$. In the following we focus on balanced heterogeneous networks, although the expressions are applicable more generally as g and ν_{ext} vary.

III. FRACTIONAL FOKKER-PLANCK EQUATION AND CONSTRUCTION OF BOUNDARY CONDITIONS

By applying the theory of Lévy processes, we obtain the membrane potential probability density $P(V, t)$ corresponding to Eq. (7), which satisfies a fractional Fokker-Planck equation [45]

$$\tau \frac{\partial P(V, t)}{\partial t} = -D_L \sigma^\alpha(t)(-\Delta_V)_\beta^{\alpha/2} P(V, t)$$
$$+ \frac{\partial}{\partial V}\{[V - \mu(t)]P(V, t)\}, \qquad (9)$$

where

$$-(-\Delta_V)_\beta^{\alpha/2} = -(-\Delta_V)^{\alpha/2} - \beta \tan \frac{\pi\alpha}{2} \frac{\partial}{\partial V}(-\Delta_V)^{(\alpha-1)/2}$$
$$(10)$$

is the skewed fractional Laplacian, and

$$(-\Delta_V)^{\alpha/2} P(V, t) = F_k^{-1}\{|k|^\alpha F_V[P(V, t)]\} \qquad (11)$$

is the fractional Laplacian, defined as a Fourier multiplier. The right-hand side of Eq. (9) consists of a fractional diffusive term arising from the fluctuations of the input, along with a drift term from the average part of the input. Since $-\Delta_x = -\frac{\partial^2}{\partial x^2}$, the equation can be rewritten as a continuity equation,

$$\frac{\partial P(V, t)}{\partial t} = -\frac{\partial S(V, t)}{\partial V}, \qquad (12)$$

where

$$S(V, t) := -\frac{D_L \sigma^\alpha(t)}{\tau} \mathcal{L}_V^{\alpha, -1} P(V, t) - \frac{V - \mu(t)}{\tau} P(V, t)$$
$$(13)$$

is the probability current through V at time t, and

$$\mathcal{L}_V^{\alpha, -1} := \frac{\partial}{\partial V}(-\Delta_V)^{(\alpha-2)/2} - \beta \tan \frac{\pi\alpha}{2}(-\Delta_V)^{(\alpha-1)/2} \quad (14)$$

has the property $\frac{\partial}{\partial V} \mathcal{L}_V^{\alpha, -1} = -(-\Delta_V)_\beta^{\alpha/2}$.

In order to map the spiking behavior of neurons onto the fractional Fokker-Planck equation (9), the boundary conditions need to be specified at the reset potential V_r and threshold θ, along with a normalization condition. In the conventional Fokker-Planck framework, neural spiking has been defined as first arrival to the threshold θ. The firing of the neuron thus imposes a point sink term $\nu(t)\delta(V - \theta)$ [19] at the threshold θ, where probability density is actively removed with rate $\nu(t)$; this is illustrated in the schematic in Fig. 1(c). Neurons exiting the refractory period are injected back into the probability density using a point source term $\nu(t - \tau_{rp})\delta(V - V_r)$ at the reset potential V_r. This injection happens at a rate equal to the firing rate of the network when those neurons had just fired, $\nu(t - \tau_{rp})$.

In our fractional case, however, the situation is more nuanced due to the discontinuous large jumps of the membrane potential $V(t)$ inherent to Lévy processes, which are absent in the continuous Gaussian trajectories. This allows the membrane potential to jump over the boundary without arriving at it; as a result, the first passage of the membrane potential $V(t)$ through the threshold θ is no longer necessarily equivalent with the first arrival of $V(t)$ at θ [see Fig. 1(d)] [35]. This

poses a problem with using the conventional Fokker-Planck derivation of absorbing boundary conditions in the fractional case. If neural spiking is still defined as first arrival to the threshold θ, then the membrane potential $V(t)$ may spend time above the threshold before firing, which is unphysical in our network model. In order for the neuron to correctly fire whenever the membrane potential is found to be above threshold, one must define neural spiking to be first passage rather than first arrival with respect to the threshold θ. Since first arrival equals first passage in the conventional Gaussian case, the definition of neural spiking as first passage is physically consistent in both the conventional and fractional cases.

When neural spiking is defined as first passage, the sink term becomes spatially extended in the fractional case, equal at each point $V \geqslant \theta$ to the probability that the membrane potential $V(t)$ lands at V at the time of first passage through the threshold θ. In the absence of resetting, the sink term is determined by the first passage leapover density [46]. The Langevin equation (7) for the membrane potential in the balanced condition $(g, \nu_{ext}) = (\gamma^{-1}, \nu_{thr})$ corresponds to Lévy motion in a quadratic external well with absorbing boundary at its extremum. In this case, the first passage leapover density $q(V, t)$ can be obtained from a variable transformation of the leapover in the free case [46,47],

$$q(V, t) = \frac{\sin(\pi\widehat{\alpha}/2)}{\pi} \frac{(\theta - V_r)^{\widehat{\alpha}/2} e^{(1-\widehat{\alpha}/2)t/\tau}}{(V - \theta)^{\widehat{\alpha}/2}[\theta - V_r + (V - \theta)e^{t/\tau}]}$$
$$(15)$$

for $V \geqslant \theta$, where

$$\widehat{\alpha} := \alpha + \frac{2}{\pi} \arctan\left(\beta \tan \frac{\pi\alpha}{2}\right) \qquad (16)$$

is related to the positivity parameter ρ [48–50] by the identity $2\alpha\rho = \widehat{\alpha}$.

When neurons exiting the refractory period are also considered, the canonical absorbing sink [47] becomes $\nu(t) *_t [p_{FP}(t)q(V, t)]$, where $*_t$ denotes temporal convolution, and $p_{FP}(t)$ is the first passage time density of a particle driven by Lévy motion in a quadratic external well out of $(-\infty, \theta)$ starting at V_r. As time passes, an expanding region is established around the reset potential V_r, characterized by the nonequilibrium stationary state [51]. Within this region, the first passage time density in the convolution may be regarded as a δ function $p_{FP}(t) = \delta(t - 1/\nu(t))$ [47]. After a large amount of time has passed, the sink term everywhere approaches the expression $\nu(t)q(V, 1/\nu(t))$. The analytical results in this work are expressed in terms of $q(V, t)$ in order to account for the unbalanced case $(g, \nu_{ext}) \neq (\gamma^{-1}, \nu_{thr})$ when its corresponding first passage leapover density $q(V, t)$ becomes known in the statistical physics literature [32–37,46–51]. Since neurons are always reset to the same reset potential V_r, the point source term $\nu(t - \tau_{rp})\delta(V - V_r)$ due to neurons exiting the refractory period remains unchanged from the classical Gaussian case.

Next, by the definition of the integrate-and-fire neuron, $P(V, t) = 0$ for $V > \theta$, and thus by continuity

$$P(\theta, t) = 0. \qquad (17)$$

Since $P(V, t)$ is a probability distribution, it is integrable [so its spatial Fourier transform $\widehat{P}(k, t)$ is smooth]:

$$\lim_{V \to -\infty} P(V, t) = \lim_{V \to -\infty} V P(V, t) = 0 \qquad (18)$$

and satisfies the normalization condition

$$\int_{-\infty}^{\infty} P(V, t) \, dV + p_r(t) = 1, \qquad (19)$$

where $p_r(t) := \int_{t - \tau_{\rm rp}}^{t} \nu(u) \, du$ is the probability that the neuron is refractory at time t. Incorporating these boundary conditions into Eq. (9) yields an analytically tractable fractional Fokker-Planck equation for characterizing motion in the presence of absorbing barriers,

$$\frac{\partial P}{\partial t} = \nu(t - \tau_{\rm rp}) \delta(V - V_r) - \nu(t) q(V, 1/\nu(t)) - \frac{\partial S}{\partial V}. \qquad (20)$$

This equation is unique in that previous approaches to incorporating absorbing barriers in the fractional Fokker-Planck equation required the truncation of the integral form of the fractional Laplacian, preventing standard analytical methods from being used [35]. Here, however, the absorbing boundary is fully encapsulated in the extended sink term, allowing the fractional Laplacian to remain untouched and hence permitting the usage of standard techniques for its analytical solution.

IV. NETWORK DYNAMICS REVEALED BY THE FRACTIONAL FOKKER-PLANCK FORMALISM

We now show that Eq. (20) can be solved under the condition $\partial P / \partial t = 0$, in order to show the stationary network dynamics of the membrane potential distribution $P_0(V)$ and firing rate ν_0, and uncover the existence of a state at which the neural response is structurally maximal. This can be done by moving into the Fourier domain and solving the resultant ordinary differential equation, as detailed in Appendix C. We denote the variables corresponding to the time-independent solution of Eq. (20) by the addition of a 0 to their subscripts, and the omission of their time arguments; the stationary membrane potential distribution $P_0(V)$ given by Eq. (C12) is

$$P_0(V) = \frac{-\tau \nu_0 P_{0,2}(\theta)}{P_{0,1}(\theta)} P_{0,1}(V) + \tau \nu_0 P_{0,2}(V), \qquad (21)$$

where $P_{0,1}(V), P_{0,2}(V)$ are defined in Eqs. (C13) and (C14). Although the fractional diffusion theory can also be derived using other neuron models, for which the first term on the right-hand side of Eq. (1) becomes an arbitrary function of V_i, we have chosen the theoretically simplest neuron model in order to focus on the heavy-tailed heterogeneity. The stationary firing rate ν_0 can be obtained by solving the implicit equation (C19), which is

$$\frac{1}{\nu_0} = \tau_{\rm rp} + \tau \frac{P_{0,2}(\theta)}{P_{0,1}(\theta)}. \qquad (22)$$

This generalizes the classical result for the mean first passage time of an IF neuron with random Gaussian inputs to the Lévy case [10,52]. We then directly calculate the stationary membrane potential distributions [Eq. (21)] and numerically [53]

solve the stationary firing rate equation (22) using the biologically realistic parameter sets detailed in Appendix D.

Figure 2(a) shows the stationary firing rate ν_0 [see Eq. (22)] as a function of the Lévy stable index α, all other parameters such as the external firing rate being kept constant. As α decreases from the classical Gaussian value $\alpha = 2$, the probability for the membrane potential V to encounter a sequence of large jumps towards the threshold θ increases. This causes an increase to the firing rate, despite the external input rate remaining constant. However, for low α close to $\alpha = 1$, the probability for a large jump of the membrane potential away from the threshold, from which it would be difficult to recover with even moderately sized jumps, begins to become significant, causing a reduction in the firing rate. These two counteracting forces on the firing rate, arising from the strong heterogeneity of synaptic strengths, are balanced around the value $\alpha = 1.2$, representing the maximum response in activity for a given external input rate; this state is referred to as the fractional state. We have obtained all values in Fig. 2 using the biologically realistic parameter set (see Appendix D), consciously choosing to keep the external firing rate constant, in order to highlight the differences caused solely by a change in structural connectivity. Here the firing rate in the classical Gaussian regime ($\alpha = 2$) is around 18 Hz, while in the fractional regime ($\alpha = 1.2$), the firing rate rises to 54 Hz, a threefold increase due solely to the heterogeneity of the network. To see the ability of the fractional regime to maintain spontaneous activity, we reduce the external stimulus to 30% the threshold value, where the classical network becomes silent, and find that the heterogeneous network maintains a low, sustained firing rate (6.73, 3.02, 1.61 Hz for $\alpha = 1.15, 1.2, 1.25$), consistent with the conditions under which heavy-tailed dynamics appear in Ref. [27]. These results thus reveal that heterogeneous neural coupling can have profound functional advantages in neural networks.

At this point of maximal response, the membrane potential rests far from the threshold [Fig. 2(b), blue line] in contrast to the classical case, where the membrane potential hovers close to the threshold [Fig. 2(b), yellow line]. To further quantify this difference and compare with experimental results on membrane potential residuals, we calculate the skewness γ_3 of the membrane potential distribution between the reset potential and threshold, which is around -0.7 and 0.5 in the Gaussian and fractional cases respectively [Fig. 2(c), red line]. These properties of membrane potential predicted by our theory are consistent with recent whole-cell V_m measurements from the visual cortex of behaving monkeys [27], in which it has been demonstrated that V_m is far from threshold during spontaneous activity, and its distribution is skewed positively with median value $\gamma_3 = 0.72$ [27]. Although leaky integrate-and-fire neurons have a hard threshold, a feature not present in other spiking neuron models such as the exponential integrate-and-fire neuron, they remain effective in capturing the subthreshold properties of membrane potentials.

The zero density of the membrane potential distribution above threshold in Fig. 2(b) demonstrates that the absorbing boundary condition has been set up properly; when the classical first arrival point sink $\nu(t) \delta(V - \theta)$ is instead used for the boundary condition [see the schematics in Figs. 1(c) and 1(d)],
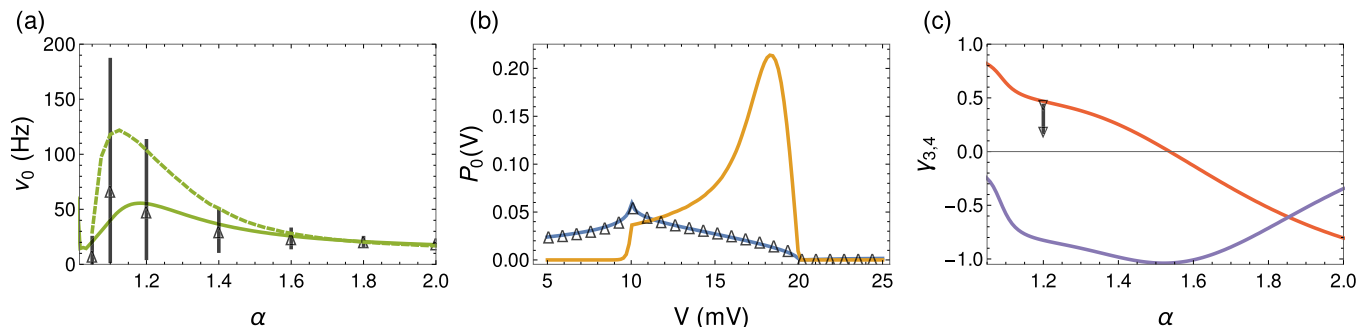
FIG. 2. Stationary states vary with the fractional Lévy index α. (a) The stationary firing rate ν_0 as a function of α under the homogeneous-rate (green) and mean-heterogeneous (green-dashed) assumptions is maximized around the optimal Lévy range $\alpha \in (1.1, 1.2)$, which is significantly higher than the firing rate arising in the classical asynchronous state ($\alpha = 2$). The vertical lines represent 5th–95th percentile ranges in the corresponding network firing rate distribution, and the triangles show their means. (b) The membrane potential distributions $P_0(V)$ for the fractional state $\alpha = 1.2$ (blue) and the Gaussian state $\alpha = 2$ (yellow) under the homogeneous-rate assumption agrees with the network values (triangles). (c) The skewness γ_3 (red) and excess kurtosis γ_4 (purple) of the membrane potential distribution under the homogeneous-rate assumption as α varies; the vertical line shows the decrease to the skewness of the network distribution when adding constant input to the network.

the membrane potential distribution in the fractional case becomes nonzero above the threshold point θ [35], representing the trajectories of the membrane potential which jump over the threshold without arriving at it.

V. SPIKING NETWORK IMPLEMENTATION

To verify our fractional diffusion theory and further illustrate that it can unify a range of neural dynamics [7,24,27], we next numerically investigate heterogeneous balanced neural networks with the distributions of heavy-tailed coupling weights approximated as power-law functions (as detailed in Sec. II).

In line with the findings in Ref. [15], we have found that when the synaptic strengths are drawn at random from their distributions [see Eq. (A15) and Appendix D], the per-neuron balance between excitation and inhibition is hindered, leading to the division of the network into silent and saturated neurons. In order to mitigate these effects, without violating the statistical independence of inputs across different populations, we ensure that the overall balance between the sums of excitatory and inhibitory connection strengths to a given neuron is sufficiently close to $g = \gamma^{-1} = 4$, so that

$$-g\gamma \sum_{i=1}^{C_E} J_{E,i} = \sum_{j=1}^{C_I} J_{I,j}. \qquad (23)$$

In our network model, we ensure tight balance for each neuron by drawing the ensembles of excitatory weights once, and then redrawing the ensembles of inhibitory weights, until the absolute ratio between the excitatory ensemble sum and the redrawn inhibitory ensemble sum is to within $\varepsilon = 10^{-3}$ of $1/g\gamma$. Importantly, we recover this balance while maintaining the heterogeneity in input connectivity.

We use the spiking neural network package NEST [54] to simulate a network of N_E excitatory and N_I inhibitory neurons; biologically realistic parameter sets (Appendix D) are used to highlight the effect of fractional, Lévy noise compared with the classical, Gaussian asynchronous irregular regime.

To represent the behavior of the fractional regime, we have chosen the value $\alpha = 1.2$, around which the firing rate response is maximized [see Fig. 2(a)]; the essential behavior of the fractional regime with respect to neural variability, however, can be seen for any α sufficiently far from the Gaussian value $\alpha = 2$. In particular, numerical simulations of network firing rates at various values of α [Fig. 2(a), triangles and vertical lines] are generally consistent with analytical predictions and demonstrate that firing rate distributions become very wide across neurons in the network in the fractional regime, which are lognormal as we explain below [see Fig. 3(c)].

To validate the prediction of our fractional diffusion theory, we compute the membrane potential distribution across all neurons in the network [Fig. 2(b), triangles], which is in excellent agreement with the theoretical stationary state values. To directly compare our results with experimental observations, we compute the per-neuron properties of membrane potentials in the fractional regime, as shown in Figs. 3(a) and 3(b). The heterogeneity in connectivity leads to a wide distribution of means and skewness of membrane potentials across neurons in the network; these heterogeneous properties across neurons are consistent with those measured in Ref. [27] [see their Figs. 2(e) and 2(f)]. Since classical, randomly connected networks with heterogeneous in-degrees are expected to have a distribution of skewness, it would be interesting to study how that skewness can be compared with quantitative data as has been done in this study.

To demonstrate how the activity of the network may be switched between the fractional state and one with more Gaussian features, as observed experimentally [27], we perform network simulations ($\alpha = 1.2$) by adding constant external input of larger magnitude. The peak of the network membrane potential distribution flattens, with its skewness decreasing from around 0.5 to 0.1 [Fig. 2(c), black], largely comparable with the decrease in skewness observed in Ref. [27] [see their Fig. 3(d)] after stimulus onset. This change can be analytically explained using the fractional theory in Appendix A, by modeling the external input as a subpopulation with
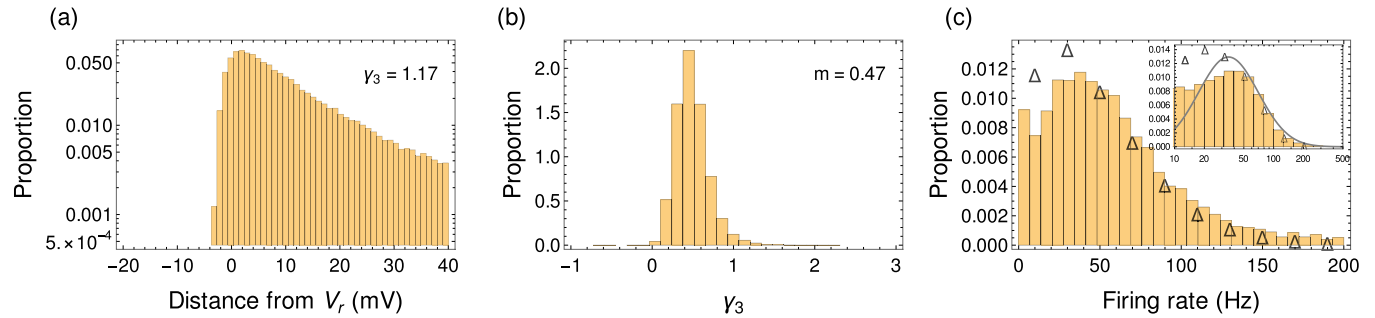
FIG. 3. Per-neuron properties of the stationary fractional state ($\alpha = 1.2$). (a) The distribution of distances of the mean membrane potential from the reset potential V_r across neurons has skewness $\gamma_3 = 1.17$. (b) The distribution of membrane potential skewness across neurons has median value $\gamma_3 = 0.47$. (c) Firing rate distribution using the Monte Carlo method applied to the mean-field formalism in Appendix B (histogram), and corresponding network distribution (triangles); lognormal fit in inset.

heterogeneity index $\alpha = 2$, while maintaining the $\alpha = 1.2$ index of the internal network subpopulations.

Next, we calculate the distribution of firing rates across neurons in the heterogeneous network; in our fractional regime, the network displays a lognormal firing rate distribution [Fig. 3(c), triangles], negatively skewed as in Refs. [12,55], but with the in-degrees C_E, C_I, C_{ext} remaining constant throughout the network. The mechanism behind this heterogeneous, lognormal firing rate behavior is the highly variable Lévy input that each neuron receives, arising from the independent, heterogeneous structure of the synaptic strengths; those neurons with a weak ensemble of synaptic strengths fire least often, while neurons with strong synaptic strength ensembles have a highly tense excitation-inhibition balance, and consequently have the highest firing rates. The skewed property of the distribution arises from the existence of a membrane time constant in the network, as noted by previous studies [12]. Classical models can robustly generate lognormal firing rate distributions by using randomly connected networks, such as Erdős-Rényi networks with constant connection probability [12–14], without requiring a tight balance condition such as Eq. (23). This is because the two sides of Eq. (23) differ by at most a Gaussian quantity in these classical models, instead of one with a power-law tail in the heterogeneous case without tight balance. Here, however, we have achieved lognormal firing rates in a model where the in-degree is constant. This is in order to isolate power-law inputs arising from network heterogeneity as a mechanism for lognormal firing rates, in conjunction with a variety of experimental findings described in this section.

To assess the ability of the fractional diffusion theory to reproduce firing rate distributions for strongly heterogeneous networks, we perform Monte Carlo simulations based on the mean-field formulation of heterogeneous firing rates under the fractional theory, in Appendix B, which proposes an additional quenched source of variability μ_q to the mean input $\mu(t)$ [Eq. (B10)]:

$$\mu_q = J\Big[\sqrt{C_E(1+\gamma g^2)\text{Var}(\nu)}W + C_{\text{ext}}^{1/\alpha}\nu_{\text{ext}}U_{\text{ext}} + (C_E\langle|\nu_\alpha|^\alpha\rangle)^{1/\alpha}U_\alpha\Big], \quad (24)$$

and find that the skewed lognormal behavior of the network is reproduced in essence [Fig. 3(c), histogram]. However, as discussed at the end of Appendix B, a significant contribution

arises due to local effects (via individual properties of nearby-connected neurons) in the strongly heterogeneous case, which are by assumption dropped in the mean-field formalism. This contribution is clearer when computing fixed points by iterating the Monte Carlo simulations [Fig. 2(a), green-dashed]: the additional correlations discussed in Appendix B serve to restrain the firing rate, but do not change its relative behavior as a function of structural connectivity α. In particular, our fractional diffusion formalism is able to capture the network peak of the firing rate at $\alpha = 1.1$ compared to the $\alpha = 1.2$ prediction under the balance condition (8) in the sense of Ref. [15].

The spikes of neurons exhibit great variability, as shown in the raster plot [Fig. 4(a)]. To quantify such variability, we calculate the coefficients of variation (CV) of the interspike interval (ISI), and find that the distribution of CV is wide in the fractional regime (Fig. 5), ranging between 0.5 and 2.5 with a mean of 1.4. On the other hand, the CVs of the classical homogeneous network with constant in-degree C_E are concentrated around a single CV value (1.0). This variability in CV arises because the ensemble sums of heterogeneous synaptic strengths in the fractional regime, while balanced across different populations, differ on a per-neuron basis, leading to vast fluctuations in firing activity across different neurons. The distribution of CVs in classical networks such as those in Ref. [12] is also broad due to the in-degree heterogeneity.

As shown in Fig. 4(a), firing rates exhibit large fluctuations over long timescales in the fractional regime. To quantify such firing rate fluctuations, as in Ref. [24], we compute the Fano factor $F(T) = \text{Var}(N(T))/\langle N(T)\rangle$ with different time window sizes T, where $N(T)$ is the individual neural spike count in time window T (Fig. 6). The fractional regime shows that for $T > 10$ ms, the Fano factor increases in a fractal manner as T increases, indicating the presence of great firing rate fluctuations. Such fluctuations can actually be fitted as power-law functions as found in Refs. [24,26]. The power-law index of the Fano factor around the optimal parameter $\alpha = 1.2$ is approximately 0.5 (Fig. 6, black dashed line), consistent with experimental findings on the firing activity of cortical neurons [26]. As noted in previous studies [56], the Fano factors in the classical asynchronous state $\alpha = 2$ have the Poisson-like value of unity only when there is no refractory period, with sub-Poisson behavior in the presence of refractory effects; however, the fractional state is able to
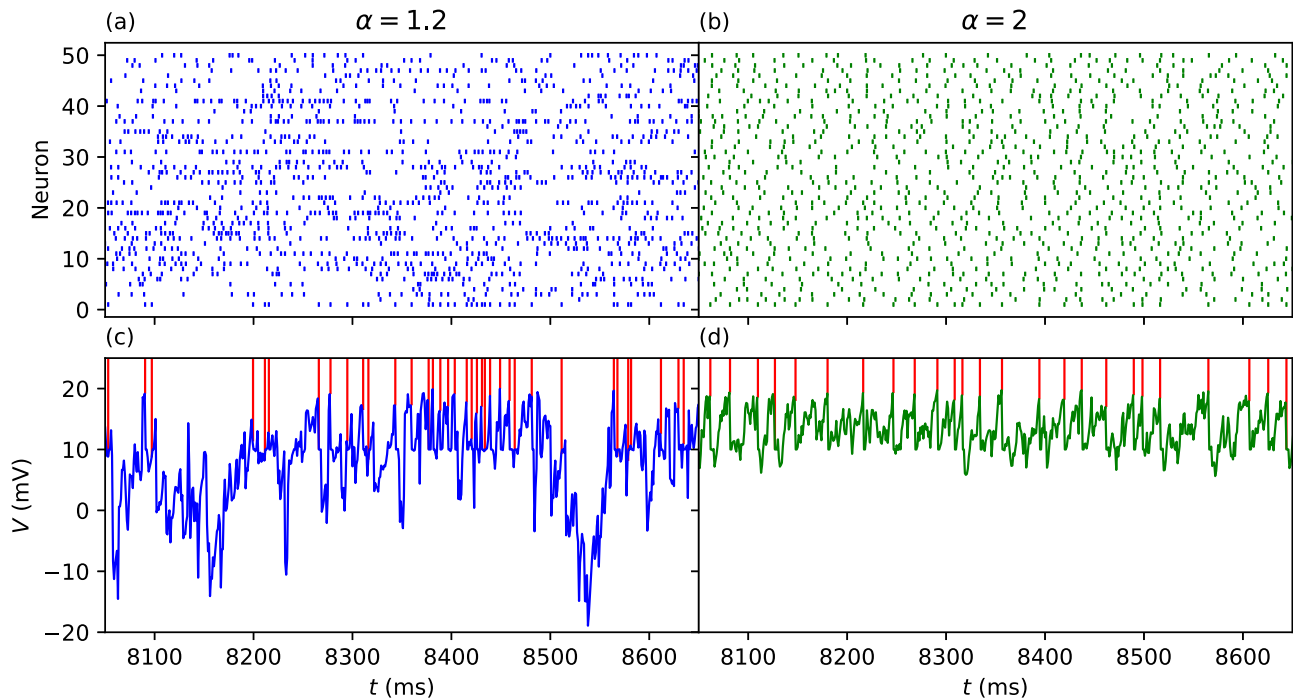
FIG. 4. Network activity in the fractional ($\alpha = 1.2$) and classical asynchronous ($\alpha = 2$) regimes. Raster plot (top) of 50 randomly chosen excitatory neurons from the network model simulation. Membrane potential time series $V(t)$ (bottom) of a single network neuron as a function of time t.

exhibit a power-law increase in the Fano factor regardless of the existence of refractory effects. This suggests the existence of a phase transition between the Gaussian and fractional

regimes, at which the long-term Fano factor switches from zero to infinity respectively [57].

To directly compare with the fluctuations of firing rates found in Ref. [7], we then calculate the variance and mean of the spike count over 1 sec windows, with each neuron
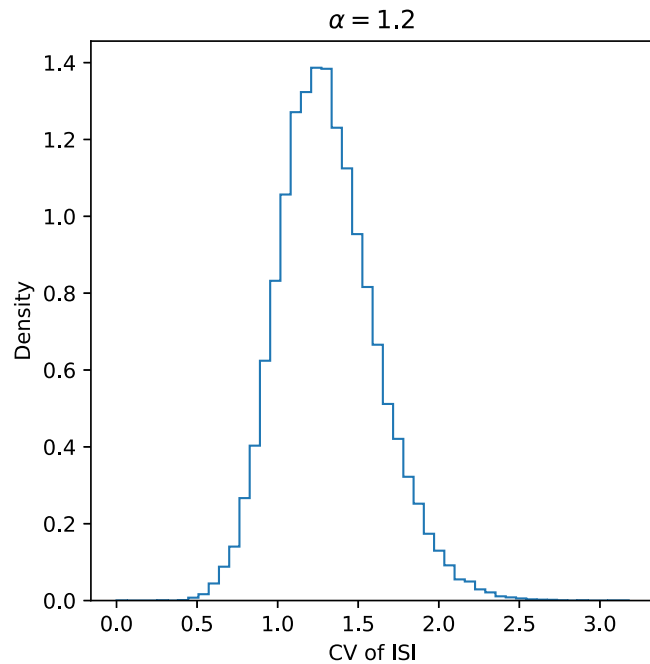

FIG. 5. Density histogram of the coefficient of variation (CV) of the interspike interval (ISI) across neurons in the heterogeneous network. The fractional regime (blue) has a wide distribution of CVs compared to the classical asynchronous regime.
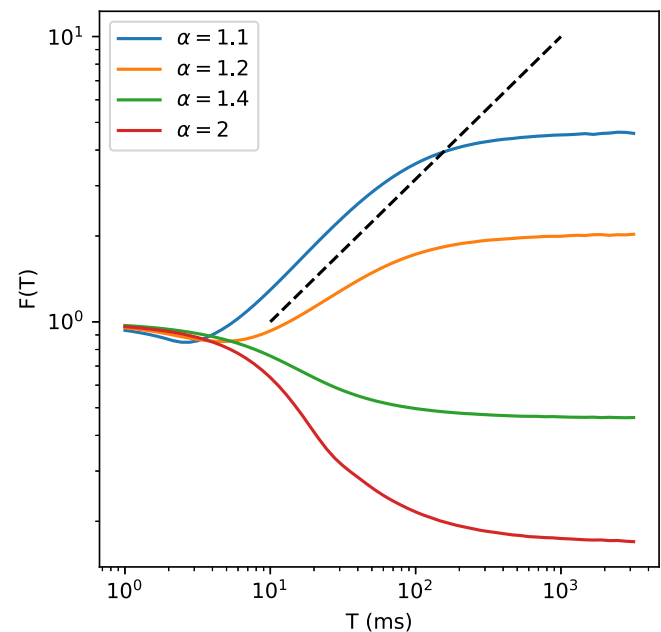

FIG. 6. Fano factor $F(T)$ of single-neuron spiking activity in the heterogeneous network as a function of time window T. Black dashed power-law line with exponent 0.5 shown for comparison.
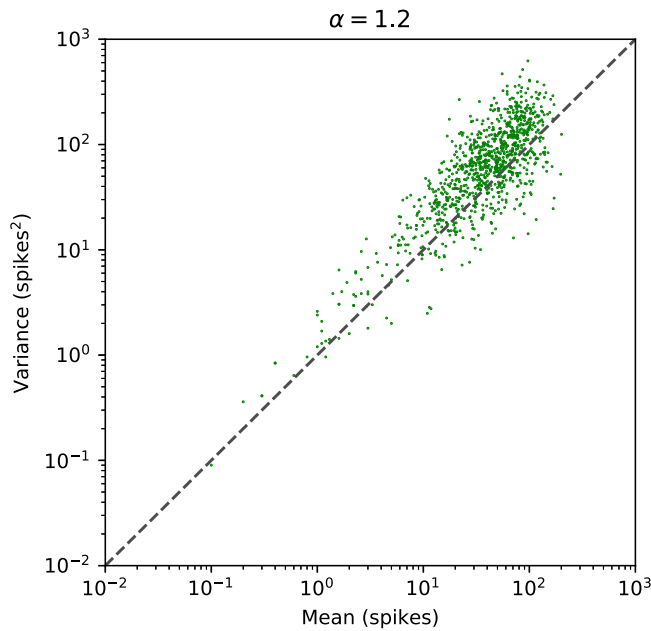
FIG. 7. Variance-to-mean relation of the neural responses to a random sample of 1000 excitatory neurons in the balanced heterogeneous network.

constituting a single data point. As shown in Fig. 7, the superlinear increase of the spike count variance as a function of its mean is consistent with experimentally observed spike count variability (see Fig. 2 in Ref. [7]) in macaque cortical areas V1, V2, and MT. In Ref. [7] such fluctuations were modeled based on a phenomenological doubly stochastic model, in which spikes are generated by a Poisson process whose rate is modulated by a slowly fluctuating gain with Gaussian dynamics. However, in our theoretical framework, such firing activity is an emergent, intrinsic property of our biologically realistic, balanced heterogeneous networks. Moreover, the doubly stochastic scenario of Ref. [7] leads to a linear scaling of the Fano factor with time window size: from Eq. (3) of Ref. [7], $F(T) = \text{Var}(N(T))/[f(S)T] = 1 + \sigma_G^2 f(S)T$, where $f(S)$ is a function of the stimulus and G is a stimulus-independent gain. This is in contrast to the power-law scaling of the Fano factor predicted by our model (Fig. 6).

We next investigate the fluctuations of population firing rate, which is the ratio between the number of spikes across the network and the time window (1 ms) over which the spikes are counted. We use the analytic Morse wavelet to compute the continuous wavelet transform and obtain the wavelet spectrogram of the population firing rate. In the fractional regime $\alpha = 1.2$, the classical observed frequency band of oscillation deteriorates, with intermittent bursting activity at all frequency scales [Fig. 8(a)]. In the classical homogeneous regime $\alpha = 2$, oscillations exist at the characteristic frequency, albeit partially suppressed in the asynchronous irregular state as shown in Fig. 8(a). Frequencies sufficiently far from the characteristic oscillation frequency are fully suppressed compared to the heterogeneous network regime. The power spectrum of the network activity displays $1/f$-like behavior in the fractional regime [Fig. 8(b)],
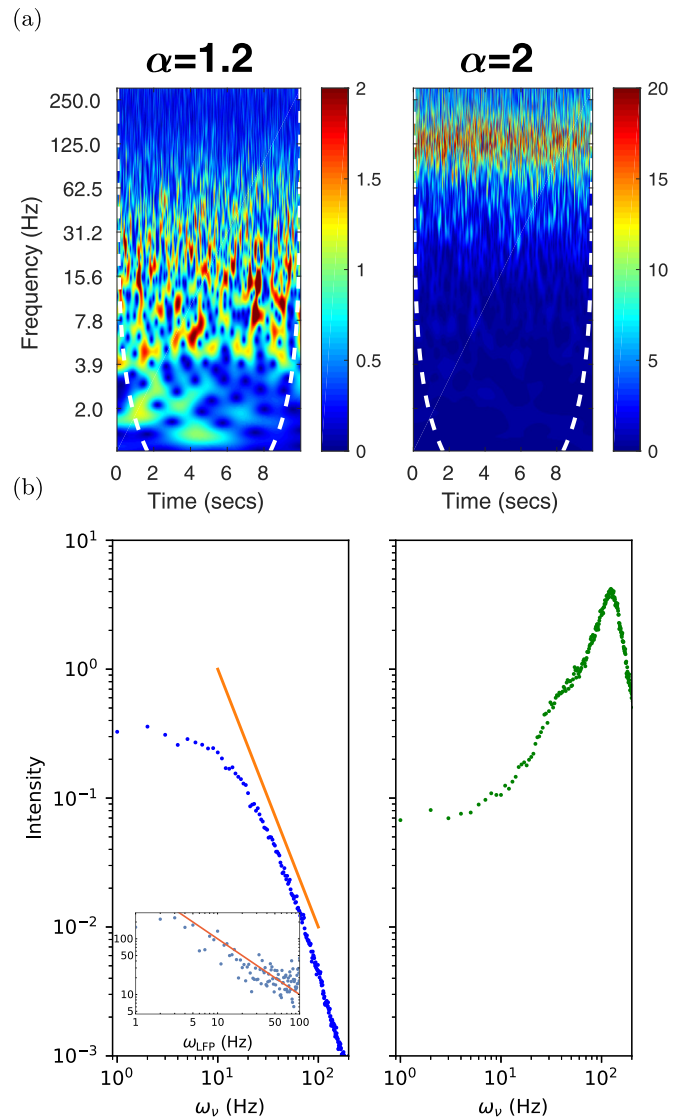

FIG. 8. (a) Wavelet spectrogram of network population firing rate as a function of time t and oscillation frequency ω, for the fractional state, $\alpha = 1.2$ (left), and the classical asynchronous state, $\alpha = 2$ (right). (b) Power spectrum (blue dots) of network population firing rate as a function of oscillation frequency ω, for $\alpha = 1.2$ (left) and $\alpha = 2$ (right). Power-law line (orange) with exponent -2.0 provided for comparison. LFP power spectrum with power-law line of exponent -1.0 in inset.

with a power-law exponent around -2.0 as observed experimentally [25,39]. Such $1/f$-like behavior can also be found using other measures for the activity of the network, such as the local field potential (LFP) calculated as the sum of the total excitatory current and the magnitude of the total inhibitory current [58]. We compute the LFP for the network model with constant external input, which exhibits the $1/f$ property [Fig. 8(b), inset]. Such fluctuations of LFPs are thus an intrinsic property of the heterogeneous network; in the conventional balanced network, an external source of fluctuations, such as an Ornstein-Uhlenbeck process with a slowly varying time constant, needs to be incorporated in order to model LFP fluctuations [59]. This scale-free behavior

of the firing rate oscillations demonstrates that the classical linear stability analysis is inadequate in the description of neural behavior around the stationary state for the fractional regime: a strongly nonlinear oscillatory response is observed in the activity with no characteristic oscillation frequency scale. This distinguishes it from both the asynchronous and synchronous irregular classical Gaussian regimes in the sense of Refs. [9,10], where (possibly partially suppressed) oscillations at characteristic frequencies continue to exist.

VI. DISCUSSION

In this study, we have developed a fractional diffusion theory of balanced, heterogeneous neural networks. By theoretically capturing the highly fluctuating, heterogeneous synaptic inputs to neurons, our theory identifies a type of state that exhibits rich nonlinear response properties, providing a unified network mechanism for a great variety of neural dynamics ranging from the individual-neuron to the network levels [5,7,25–27], which otherwise remain disjointed in existing theories and models. Importantly, in this state the neural response is maximized as a function of structural connectivity; i.e., the firing rate for a given external input is at its greatest.

The fractional diffusion theory provides a theoretical framework for understanding how complex neural dynamics can emerge from heterogeneous networks. In this theory, fluctuating synaptic inputs to neurons are formulated as Lévy stochastic processes. These Lévy processes are characterized by intermittent large jumps; the presence of these processes is a hallmark of nonequilibrium complex systems [32–37]. In our theory, we rigorously demonstrate that these processes arise from heterogeneous neural networks in which the synaptic coupling weights are heavy-tailed and comparable with the size of the network. In the large network size limit, as a result of the generalized central limit theorem, this corresponds to heavy-tailed, power-law weights. This is, however, fundamentally different from recent studies of heterogeneous neural networks, in which heterogeneous connectivity has been interpreted in terms of heavy-tailed degree distributions with [18] and without [15] heavy-tailed synaptic strength distributions. Some of the discussed experimental phenomena can be reproduced using a different variant of the classical model with Gaussian input statistics. For example, up-down fluctuations in membrane potential can be accounted for by incorporating adaptation into the classical models [28], while $1/f$-fluctuations of LFPs and super-Poissonian features of neural activity can be generated by adding a time-varying component to the network inputs [7,59]. The strength of the fractional theory is that these, along with other currently unexplained phenomena such as the power-law increase of the Fano factor over time window [24] and the infrequent large fluctuations of membrane potential [27], can be explained in a single framework. As for the specific network model considered in this study, the tight balance condition (23) is used in simulations to avoid the disruption of excitation-inhibition balance by the network heterogeneity, consistent with that observed in Ref. [15]. This tight balance condition appears to be biologically implausible; however, it may be naturally recovered using neural mechanisms discussed in Ref. [15], such as homeostatic plasticity or spike-frequency adaptation.

In our theory, the Lévy statistics allows for an application of fractional diffusion formalisms in neural networks. Previous studies of fractional diffusion in various branches of statistical physics [35] have encountered difficulties when attempting to use the fractional Fokker-Planck equation in the presence of absorbing boundaries. The integral truncations performed in those studies on the fractional Fokker-Planck operator to incorporate these boundary conditions break its convenient Fourier multiplier representation, rendering it unusable for analytical predictions. To develop an analytically tractable fractional Fokker-Planck equation with the required absorbing boundary conditions in neural networks, we construct a link between the first passage time and the first passage leapover, previously regarded as related but independent concepts [46,47]. Our unique fractional formalisms can thus be used to analytically reveal the circuit mechanism of complex neural dynamics, extending the recent interest in using fractional approaches for understanding complex physical systems [31,60] to a new area.

Occasional, large synaptic inputs which are the hallmark features of Lévy processes have been found in neural circuit models, due to a combination of heavy-tailed but non-power-law connectivity features along with a specific dynamical state of the circuit [18], e.g., near a transition regime between different circuit states. We thus expect that the fractional diffusion theory applies whenever the inputs have Lévy fluctuations, regardless of specific network structures. In addition, it should be noted that scale-free, Lévy-like fluctuations can emerge from neural networks with criticality [3,18,61,62]. In the future it would be interesting to apply our fractional framework for the formulation of critical neural dynamics, going beyond the demonstration of the presence of heavy-tailed distributions in some neural observables.

As we have demonstrated, our fractional theoretical framework provides a unified account of key properties of neural activity at the individual-neuron and the circuit levels. First, membrane potentials in our model exhibit non-Gaussian dynamics, consisting of quiescent periods interrupted by short intervals of high-amplitude depolarization, and reside far from the threshold. Such non-Gaussian fluctuations of membrane potential have been observed in the spontaneous activity of cortical neurons [27] but are inconsistent with the existing random walk models [63], which instead predict Gaussian dynamics of membrane potential. Large fluctuations of membrane potential could be obtained from classical excitatory-inhibitory balanced networks with a suitable choice of parameters, leading to Gaussian statistics with frequent fluctuations on the order of the standard deviation. However, the infrequent, occasional large spontaneous fluctuations observed in Ref. [27] cannot be compatible with Gaussian input statistics, as noted in Ref. [27], but can be captured in our model. Moreover, while the classical excitatory-inhibitory spiking circuits have been able to account for the fluctuations of up- and down-states of membrane potentials, which have often been observed in cortex of anesthetized animals, by incorporating additional mechanisms such as adaptation [28], the fractional diffusion theory is mainly used in this study to explain the brief, large excursions of membrane potential dynamics observed in awake cortex [27,64]. The non-Gaussian state in Ref. [27], which

occurs during awake fixation, is characterized by infrequent, brief bumps in inputs, which constitute a defining feature of the Lévy process.

Second, the variance of spike counts is a super-linear function of their mean as measured in Ref. [7], and the Fano factor of spike counts increases as a power-law as a function of the time window, as found in Refs. [24,26]. In contrast, in the classical normal diffusion theory, the variance of spike counts is equal to the mean, and the Fano factor remains constant over large timescales. Phenomenological models based on the Poisson process with the incorporation of global fluctuating modulation factors have been proposed to account for such fluctuations of firing activity [7]. However, as we mathematically demonstrate in the Results, such super-Poisson statistics display a linear scaling of the Fano factor of spike counts over time window. Furthermore, because the sources of these global fluctuations are in general unknown, these phenomenological models are somewhat circular, leaving the fundamental problem of the circuit mechanism underlying the fluctuations unaddressed. While super-Poisson statistics of neural firing activity can emerge from some spiking neural circuits [56,65–67], analyses of their Fano factor of spike counts also suggest that it scales linearly over time window. However, in our model, the Fano factor increases as a power law with time window, as found in experimental studies [24,26]. By demonstrating that such firing rate fluctuations are an intrinsic property of our heterogeneous balanced circuits, our study identifies a circuit mechanism by which these phenomena can be explained.

Third, firing rates across neurons are highly heterogeneous, with some neurons firing a lot but others firing much less, resulting in the heavy-tailed lognormal distribution as widely observed in experimental studies [23]. Fourth, the population firing rate and local field potentials in the fractional state oscillate across multiple frequency scales in a $1/f$ manner, and all oscillations, such as gamma oscillations at 40 Hz, occur intermittently in a bursting manner, consistent with experimental studies of population activity recorded by local field potentials [25,39]. Achieving such nonlinear behaviors of oscillations in conventional balanced neural networks has remained a major challenge, due to the presence of a single characteristic frequency as predicted by the linear stability analysis in the conventional Fokker-Planck formalism [10,38].

Our theory identifies a state of activity in which the response of the circuit to input is nonlinear and structurally maximal. Due solely to the heterogeneity of the network, the neural response for the same average input is significantly higher than that of the classical asynchronous state, and in the fractional state, the stationary firing rate is maximal as a function of the fractional Lévy index α arising in the synaptic strength distribution. The utility of a higher firing rate response, relative to the Gaussian state, is of interest in maintaining neural firing during spontaneous activity [27], which we confirm in the Results. For the remainder of our investigations, in order to ensure that any differences observed in the fractional state truly arise from changes in structural connectivity, we have kept the physiological parameters of the network, such as the excitatory-inhibitory balance, the external input size, the mean connection strength, and the mean in-degree, unchanged from the classical case. These,

combined with recent results on enhanced responsiveness due to the heterogeneity of inhibitory neurons [68], indicate that network structure has a fundamental impact on the dynamics of neural activity. In this fractional regime, other variability properties remain consistent with physiological findings; this drives us to use the term 'regime' to capture a range of nonlinear, nonequilibrium phenomena which cannot be obtained solely by changing other physiological, magnitude-based constraints.

To test this structurally maximal regime with the essentially nonlinear computation properties revealed in our study, it would be ideal to combine intra- and extra-cellular recordings with massive multi-unit recordings in order to measure the fluctuations of membrane potentials and firing activity at the individual neuron and population levels. This could be done in conjunction with the analysis of membrane potential, synaptic input and neural fluctuations by using the same methods as we have done in our modeling study.

APPENDIX A: DERIVATION OF LÉVY STABLE INPUT

To demonstrate the emergence of Lévy stable input, we consider a single neuron in a network undergoing a discrete time evolution with time step Δt, so the probability of a neuron in population r being active at a given time step is $\langle s(t) \rangle_r := \nu_r(t - D)\Delta t$. The probability that a neuron receives a connection from a given neuron in population r is C_r/N_r. The general idea here is to consider the inputs from each population of incoming neurons separately, and use the properties of stable processes to combine them into the total input. The outgoing connection strengths from population r are drawn from a distribution characterizing the random variable J_r. If X_r is the random variable representing the firing of an incoming neuron from population r, which is Bernoulli with probability λ_r/N_r, where $\lambda_r := C_r \langle s(t) \rangle_r$, then the characteristic function of $J_r X_r$ is

$$\varphi_{J_r X_r}(u) = \langle \varphi_{X_r}(u J_r) \rangle_{J_r} \tag{A1}$$

$$= \left\langle 1 - \frac{\lambda_r}{N_r} + \frac{\lambda_r}{N_r} e^{iu J_r} \right\rangle_{J_r} \tag{A2}$$

$$= 1 - \frac{\lambda_r}{N_r} + \frac{\lambda_r}{N_r} \varphi_{J_r}(u), \tag{A3}$$

generalizing the characteristic function of a Bernoulli random variable. Suppose now that X_i, J_i are independent and distributed as X_r, J_r, for all $i = 1, \ldots, N_r$. The characteristic function for the total synaptic input to the neuron from population r is

$$\varphi_{\sum_{i=1}^{N_r} J_i X_i}(u) = \prod_{i=1}^{N_r} \varphi_{J_i X_i}(u) \tag{A4}$$

$$= \varphi_{J_r X_r}(u)^{N_r} \tag{A5}$$

$$= \left[1 - \frac{\lambda_r}{N_r} + \frac{\lambda_r}{N_r} \varphi_{J_r}(u) \right]^{N_r} \tag{A6}$$

$$= \left\{ 1 + \frac{\lambda_r [\varphi_{J_r}(u) - 1]}{N_r} \right\}^{N_r} \tag{A7}$$

$$\xrightarrow{N_r \to \infty} e^{\lambda_r [\varphi_{J_r}(u) - 1]} \tag{A8}$$

generalizing the Poisson limit theorem. Then, using Lévy's continuity theorem [44],

$$\varphi_{\sum_{i=1}^{\infty} J_i X_i}(u) = e^{\lambda_a [\varphi_{J_r}(u)-1]} \tag{A9}$$

$$= (e^{\varphi_{J_r}(u)-1})^{\lambda_r} \tag{A10}$$

$$= \varphi_{\sum_{j=1}^{\lambda_r} Y_j}(u), \tag{A11}$$

where λ_r is taken to be an integer in the last equality (valid for large λ_r), and the Y_j are iid random variables with $\varphi_{Y_j}(u) = e^{\varphi_{J_r}(u)-1}$. The cumulant generating function (second characteristic function) of Y_j is

$$H_{Y_j}(u) = \ln \varphi_{Y_j}(u) \tag{A12}$$

$$= \varphi_{J_r}(u) - 1, \tag{A13}$$

so the cumulants of Y_j are precisely the moments of J_r; in particular, $\langle Y_j \rangle = \langle J_r \rangle$.

The remainder of the derivation is split into two cases: when the second moment (or equivalently, the variance) of J_r is infinite, and when it is finite. We consider first the former case. Suppose that the random variable J_r satisfies

$$\varphi_{J_r}(u) \sim 1 - D_r |\langle J_r \rangle u|^\alpha \tag{A14}$$

as $u \to 0$, so that its probability density function has a positive tail of the form

$$p_{J_r}(x) \sim 2 A_\alpha D_r |\langle J_r \rangle|^\alpha |x|^{-\alpha-1} \tag{A15}$$

as $x \to +\infty$, where $A_\alpha = \Gamma(1+\alpha)\sin(\pi\alpha/2)/\pi$ [69, pp. 10–11] is a constant independent of the population, and a negative tail which decays more rapidly. Then, using the generalized central limit theorem [44],

$$\lambda_r^{-1/\alpha} \sum_{j=1}^{\lambda_r} Y_j \bigg|_{\lambda_r \to \infty} = L\left(\alpha, 1, \left\langle \lambda_r^{-1/\alpha} \sum_{j=1}^{\lambda_r} Y_j \right\rangle, D_r |\langle J_r \rangle|^\alpha \right). \tag{A16}$$

If, instead, the connection strengths of the population have a dominant negative tail (e.g. the inhibitory population), the above holds with the exception of the skew parameter β_r taking the value -1. Hence, using the additive property of the stable law, the total synaptic input to the neuron from all populations is

$$\sum_r \sum_{i=1}^{\infty} (J_i X_i)_r \bigg|_{\lambda_r \to \infty}$$

$$= \sum_r \sum_{j=1}^{\lambda_r} Y_j \bigg|_{\lambda_r \to \infty} \tag{A17}$$

$$= \sum_r L(\alpha, \beta_r, \lambda_r \langle J_r \rangle, \lambda_r D_r |\langle J_r \rangle|^\alpha) \tag{A18}$$

$$= L\left(\alpha, \beta, \sum_r \lambda_r \langle J_r \rangle, \sum_r \lambda_r D_r |\langle J_r \rangle|^\alpha \right) \tag{A19}$$

$$= \sum_r \lambda_r \langle J_r \rangle + \left(\sum_r \lambda_r D_r |\langle J_r \rangle|^\alpha \right)^{1/\alpha} L(\alpha, \beta, 0, 1), \tag{A20}$$

where $\beta = \frac{\sum_r \beta_r \lambda_r D_r |\langle J_r \rangle|^\alpha}{\sum_r \lambda_r D_r |\langle J_r \rangle|^\alpha}$. Moving into the continuous-time limit, one obtains

$$I_i(t)\, dt = \tau \sum_r C_r \nu_r(t - D)\langle J_r \rangle\, dt$$

$$+ \tau \left[\sum_r C_r \nu_r(t - D) D_r |\langle J_r \rangle|^\alpha \right]^{1/\alpha} dL(\alpha, \beta, 0, 1). \tag{A21}$$

If all populations have the same coefficient $D_r = D_L$, then

$$I_i(t)\, dt = \tau \sum_r C_r \nu_r(t - D)\langle J_r \rangle\, dt$$

$$+ \tau \left[\sum_r C_r \nu_r(t - D) |\langle J_r \rangle|^\alpha \right]^{1/\alpha} dL(\alpha, \beta, 0, D_L). \tag{A22}$$

Since $C_I = \gamma C_E$, the skew parameter of the noise in our excitatory-inhibitory network model becomes

$$\beta = \frac{(1 - \gamma g^\alpha)\nu(t - D) + \nu_{\text{ext}}}{(1 + \gamma g^\alpha)\nu(t - D) + \nu_{\text{ext}}}. \tag{A23}$$

In the latter case, when J_r has finite second moment, the generalized central limit theorem reduces to the regular central limit theorem and $\alpha = 2$. Choose D_r such that

$$\frac{\langle J_r^2 \rangle}{2} = D_r |\langle J_r \rangle|^2. \tag{A24}$$

Since the second moment of J_r is equal to the second cumulant (the variance) of Y_j, the above derivation for $1 < \alpha < 2$ extends to the $\alpha = 2$ case with Eqs. (A14) and (A15) replaced by Eq. (A24).

The generalized central limit theorem, in the form stated in Table 2.1 of Ref. [44], allows for another case (not investigated in this study). When $p_{J_r}(x) \sim 2 D_r |\langle J_r \rangle|^2 |x|^{-3}$ (note the absence of the A_α term) the resultant dynamics of the model become Gaussian again, with the sole change being the replacement of the $x_r := C_r \nu_r(t - D_B)$ term in $\sigma(t)$ with $x_r \log x_r$.

Note that both the central limit theorem and its generalized variant rely on the synaptic strength distribution J_r having a well-defined asymptotic tail. As a result, some finite networks

with non-power-law empirical synaptic strength distributions may in fact belong to the Lévy universality class if these empirical distributions do not retain their finite-size behavior in the large network limit. We leave the elucidation of the consequences of the asymptotic tail assumption to future work.

APPENDIX B: LÉVY STABLE INPUT WITH HETEROGENEOUS FIRING RATE DISTRIBUTIONS

In this section we demonstrate how the fractional mean-field theory in Appendix A may be extended to predict distributions of population firing rates. In the classical theory, where the firing rate, synaptic strength, and number of connections all had finite variance across the network, this involved adding a quenched Gaussian term to the mean input $\sum_{i=1}^{C_r} v_{r,i} J_{r,i}\, dt$ for each population r. This corresponds to the first term on the right-hand sides of Eqs. (A20) and (A21). Due to the Gaussian randomness, it was sufficient to perform this to first order for each of these sources of randomness [12–14,70].

In the fractional diffusion theory, the same technique would yield a firing rate distribution describing the network in the absence of the tight balance condition (23). However, incorporating this balance condition causes the first-order terms to cancel out for the internal populations, and the analysis for these populations must then be brought to second order.

Using the generalized central limit theorem and the synaptic heavy-tailed assumption (A15), the mean input arriving from population r to a randomly selected network neuron approaches, in the limit of a large number of connections,

$$\sum_{i=1}^{C_r} v_{r,i} J_{r,i}\Bigg|_{C_r \to \infty} = \langle J_r \rangle \left[\sum_{i=1}^{C_r} v_{r,i} + \left(C_r \langle v_r^\alpha \rangle \right)^{1/\alpha} U_r \right] \quad (B1)$$

$$= \langle J_r \rangle \big[C_r \langle v_r \rangle + \sqrt{C_r \mathrm{Var}(v_r)}\, W_r$$

$$+ \left(C_r \langle v_r^\alpha \rangle \right)^{1/\alpha} U_r \big], \quad (B2)$$

where $v_{r,i}$ are samples drawn from the population firing rate distribution v_r; $U_r \sim L(\alpha, 1, 0, D_r)$ is a quenched α-stable sample; and $W_r \sim \mathcal{N}(0, 1) = L(2, 0, 0, 1/2)$ is a quenched Gaussian sample. When C_r is large, the central limit theorem applies on $0 \leqslant v_r \leqslant 1/\tau_{\mathrm{rp}}$ since it is bounded. This yields a closed, self-consistent system of equations to second order in the absence of tight balance.

To incorporate the balance condition (23), we observe that the above implies for the inhibitory population that

$$\sum_{j=1}^{C_I} v_{I,j} J_{I,j} = \langle J_I \rangle \sum_{j=1}^{C_I} v_{I,j} + \langle J_I \rangle \left(\gamma C_E \langle v_I^\alpha \rangle \right)^{1/\alpha} U_{I,1} \quad (B3)$$

in the limit of large C_I. Similarly, taking another C_E new samples of the product $v_I J_I$,

$$\gamma^{1/\alpha} \sum_{i=1}^{C_E} v_{I,i} J_{I,i} = \gamma^{1/\alpha} \langle J_I \rangle \sum_{i=1}^{C_E} v_{I,i} + \langle J_I \rangle \left(\gamma C_E \langle v_I^\alpha \rangle \right)^{1/\alpha} U_{I,2}, \quad (B4)$$

and we find that in distribution

$$\sum_{j=1}^{C_I} v_{I,j} J_{I,j} = \langle J_I \rangle \sum_{j=1}^{C_I} v_{I,j} - \gamma^{1/\alpha} \langle J_I \rangle$$

$$\times \sum_{i=1}^{C_E} v_{I,i} + \gamma^{1/\alpha} \sum_{i=1}^{C_E} v_{I,i} J_{I,i}. \quad (B5)$$

The tight balance condition (23) then allows us to take $J_{I,i} = -g J_{E,i}$, noting that $J_{I,i}$ are random samples of the distribution J_I which do not appear as network synaptic strengths; similarly the $v_{I,i}$ do not appear in the network as individual neural firing rates. As a result, we have that in distribution the mean input from the internal populations with tight balance is

$$\sum_{i=1}^{C_E} v_{E,i} J_{E,i} + \sum_{j=1}^{C_I} v_{I,j} J_{I,j} = \langle J_I \rangle \sum_{j=1}^{C_I} v_{I,j} - \gamma^{1/\alpha} \langle J_I \rangle \sum_{i=1}^{C_E} v_{I,i} + \sum_{i=1}^{C_E} \left(v_{E,i} - g \gamma^{1/\alpha} v_{I,i} \right) J_{E,i} \quad (B6)$$

$$= \langle J_E \rangle \sum_{i=1}^{C_E} v_{E,i} + \langle J_I \rangle \sum_{j=1}^{C_I} v_{I,j} + \langle J_E \rangle (C_E \langle |v_\alpha|^\alpha \rangle)^{1/\alpha} U_\alpha, \quad (B7)$$

where

$$U_\alpha \sim L\left(\alpha, \frac{\langle \mathrm{sgn}(v_\alpha) |v_\alpha|^\alpha \rangle}{\langle |v_\alpha|^\alpha \rangle}, 0, D_r \right) \quad (B8)$$

is a quenched α-stable sample, and $v_\alpha = v_E - g \gamma^{1/\alpha} v_I$ is a random variable. Since in our model excitatory and inhibitory neurons have identical characteristics, the distributional equality $v_E = v_I$ yields the following modification to Eq. (3) for the input $I(t)$ to a randomly selected neuron at time t:

$$I(t) = \mu(t) + \mu_q(t) + \sigma(t) \tau^{1-1/\alpha} \eta(t), \quad (B9)$$

where

$$\mu_q = J[\sqrt{C_E(1 + \gamma g^2)\mathrm{Var}(v)}\, W$$

$$+ C_{\mathrm{ext}}^{1/\alpha} v_{\mathrm{ext}} U_{\mathrm{ext}} + (C_E \langle |v_\alpha|^\alpha \rangle)^{1/\alpha} U_\alpha] \quad (B10)$$

is the quenched contribution to the mean input, and instances of $v(t)$ are replaced with their population means, $\langle v \rangle(t)$. This system of equations is closed through the definition of $\langle v \rangle(t)$, $\mathrm{Var}(v)(t)$, $\langle |v_\alpha|^\alpha \rangle(t)$, and $\langle \mathrm{sgn}(v_\alpha) |v_\alpha|^\alpha \rangle(t)$.

Finally, the above is conducted under the assumption that the firing rate of a neuron is uncorrelated with its outgoing synaptic strengths. This may no longer be the case in such strongly connected networks, especially given the propensity

for networks with rich clubs to exhibit local rather than global behavior [18]. We have attempted to account for this by assuming that neurons with low firing rates have a small sum of incoming synaptic strength magnitudes, and vice versa. However, the mean-field construction links the firing rate of a neuron with only its incoming, rather than both its incoming and outgoing, synaptic strengths. This approaches the limit of what can be achieved using such mean-field techniques: the correlations between the outgoing and incoming properties of individual elements begin to become too significant for a general mean-field analysis. Unlike the situation in Ref. [13], where the correlations between neural firing rates and their *a priori* correlated in- and out- degrees were able to be considered, the incoming and outgoing synaptic strengths in our model are independent. In the future, new techniques, possibly inspired by fractal, renormalization group-like methods, may replace the mean-field technique in describing the behavior of heterogeneous, complex systems in statistical physics.

APPENDIX C: DERIVATION OF THE STATIONARY STATES

Here we present the technical derivation of the stationary states of the system, which consists of solving a fractional differential equation. Classical analyses of FFPEs in the absence of absorbing boundary conditions tend to prefer solving the system in Fourier-Laplace space [71], where the relevant dynamical operators have a simple form. Using our analytically tractable absorbing boundary conditions, we undertake a similar method whereby we move into Fourier space, and take the inverse Fourier transform of the solution to the Fourier ordinary differential equation.

In the stationary state [where $q_0(V) := q(V, 1/\nu_0)$],

$$
0 = \nu_0[\delta(V - V_r) - q_0(V)]
$$
$$
+ \frac{1}{\tau}\left\{-D_L\sigma_0^\alpha(-\Delta_V)_\beta^{\alpha/2}P_0(V) + \frac{\partial}{\partial V}[(V - \mu_0)P_0(V)]\right\}. \tag{C1}
$$

With the aid of the following rudimentary properties of the Fourier transform of a function $f \in \mathcal{L}^p(\mathbb{R})$:

$$
F_x\left[\frac{\partial}{\partial x}f(x)\right](k) = -ikF[f](k), \tag{C2}
$$

$$
F_x[(-\Delta_x)^{c/2}f(x)](k) = |k|^c F[f](k), \tag{C3}
$$

$$
F_x[xf(x)](k) = -i\frac{\partial}{\partial k}F[f](k), \tag{C4}
$$

$$
F_x[\delta(x - a)](k) = e^{ika}, \tag{C5}
$$

where $p \in [1, 2]$ and $c \in (0, 2]$, Eq. (C1) is expressed in Fourier space as

$$
0 = \nu_0\left[e^{iV_r k} - \widehat{q_0}(k)\right]
$$
$$
+ \frac{1}{\tau}\left[-D_L\sigma_0^\alpha|k|_\beta^\alpha\widehat{P_0}(k) - ik\left(-i\frac{\partial}{\partial k} - \mu_0\right)\widehat{P_0}(k)\right], \tag{C6}
$$

where

$$
|k|_\beta^\alpha := |k|^\alpha + \beta\tan\frac{\pi\alpha}{2}(-ik)|k|^{\alpha-1} \tag{C7}
$$

$$
= |k|^\alpha\left[1 - i\beta\tan\frac{\pi\alpha}{2}\text{sgn}(k)\right] \tag{C8}
$$

is the multiplier corresponding to the skewed fractional Laplacian $(-\Delta_V)_\beta^{\alpha/2}$. The solution to this first-order differential equation is

$$
\widehat{P_0}(k) = C\widehat{P_{0,1}}(k) + \tau\nu_0\widehat{P_{0,2}}(k), \tag{C9}
$$

where

$$
\widehat{P_{0,1}}(k) = e^{ik\mu_0 - \frac{D_L\sigma_0^\alpha}{\alpha}|k|_\beta^\alpha}, \tag{C10}
$$

$$
\widehat{P_{0,2}}(k) = -i\int_0^k dk_1\, \frac{e^{ik_1 V_r} - \widehat{q_0}(k_1)}{-ik_1}
$$
$$
\times e^{i(k-k_1)\mu_0 - \frac{D_L\sigma_0^\alpha}{\alpha}(|k|_\beta^\alpha - |k_1|_\beta^\alpha)}, \tag{C11}
$$

and C is a constant determined by the boundary conditions, and so

$$
P_0(V) = CP_{0,1}(V) + \tau\nu_0 P_{0,2}(V). \tag{C12}
$$

Taking the inverse Fourier transform of Eqs. (C10) and (C11) yields expressions in terms of the standard α-stable distribution,

$$
P_{0,1}(V) = p_{L_1}(V - \mu_0), \tag{C13}
$$

$$
P_{0,2}(V) = \int_0^1 \frac{dk_2}{k_2}\left\{p_{L_2}[V - \mu_0 - k_2(V_r - \mu_0)]\right.
$$
$$
\left. - \frac{q_0(V/k_2)}{k_2} *_V p_{L_2}[V - \mu_0(1 - k_2)]\right\}, \tag{C14}
$$

where

$$
L_1 := L(\alpha, \beta, 0, D_L\sigma_0^\alpha/\alpha), \tag{C15}
$$

$$
L_2 := L(\alpha, \beta, 0, D_L\sigma^\alpha(1 - k_2^\alpha)/\alpha), \tag{C16}
$$

and $f(V) *_V g(V) = \int f(V - V_1)g(V_1)\,dV_1$ is the convolution operator. To understand the effect of the threshold θ on the solution, Eq. (C14) can be written as

$$
P_{0,2}(V) = \int_0^1 \frac{dk_2}{k_2}\left\{p_{L_2}[V - \mu_0 - k_2(V_r - \mu_0)]\right.
$$
$$
\left. - \int_\theta^\infty dV_2\, q_0(V_2)p_{L_2}[V - \mu_0 - k_2(V_2 - \mu_0)]\right\}. \tag{C17}
$$

To increase computational accuracy, the boundaries in the inner integral in Eq. (C17) can be rewritten over $\mathbb{R}$, giving

$$
P_{0,2}(V) = \int_0^1 \frac{dk_2}{k_2}\left\{p_{L_2}[V - \mu_0 - k_2(V_r - \mu_0)]\right.
$$
$$
- \int_{-\infty}^\infty e^{V_3}dV_3\, q_0(e^{V_3} + \theta)
$$
$$
\left. \times p_{L_2}[V - \mu_0 - k_2(e^{V_3} + \theta - \mu_0)]\right\}. \tag{C18}
$$

TABLE I. Parameter sets used in this paper.

	$\alpha = 1.2$	$\alpha = 2$	Units
N_E	40 000	10 000	
N_I	10 000	2500	
γ	0.25	0.25	
C_E	4000	1000	
C_I	1000	250	
C_{ext}	4000	1000	
τ	20	20	ms
D	1.5	1.5	ms
ν_{ext}	1	2	ν_{thr}
θ	20	20	mV
V_r	10	10	mV
τ_{rp}	2	2	ms
J	0.02	0.1	mV
g	4	5	

Using the two boundary conditions (17) and (19) to determine the two remaining undetermined variables ν_0 and C, one obtains $1 - \nu_0 \tau_{\mathrm{rp}} = 1 - p_{r,0} = \widehat{P}_0(0) = C\widehat{P_{0,1}}(0) + \tau\nu_0\widehat{P_{0,2}}(0) = C$ and $0 = P_0(\theta) = CP_{0,1}(\theta) + \tau\nu_0 P_{0,2}(\theta)$. Thus the self-consistent condition that determines ν_0, the stationary firing rate, is

$$0 = (1 - \nu_0 \tau_{\mathrm{rp}})P_{0,1}(\theta) + \tau\nu_0 P_{0,2}(\theta), \qquad (C19)$$

or equivalently

$$\frac{1}{\nu_0} = \tau_{\mathrm{rp}} + \tau\frac{P_{0,2}(\theta)}{P_{0,1}(\theta)}. \qquad (C20)$$

APPENDIX D: NETWORK IMPLEMENTATION DETAILS

To visualize the behavior of the system in this study, it is necessary to specify biologically realistic numerical values for the network parameters. These values are presented for the two parameter sets we use in Table I. The biologically realistic values are derived from the balanced case in Sec. 4 of Ref. [10], with a tenfold decrease in the mean excitatory connection strength J in order to produce realistic membrane potential distributions in the Gaussian regime. The parameters for the classical, asynchronous irregular case ($\alpha = 2$) are derived from Fig. 7(c) of Ref. [10].

To construct a computationally tractable synaptic strength distribution for the network satisfying Eq. (A15), we consider the lower-bound-truncated translated power-law distribution for the synaptic connection strengths,

$$p_J(x) = \frac{2A_\alpha D_L \langle J \rangle^\alpha}{|x - x_0|^{\alpha+1}} 1_{(x_0 + x_1, \infty)}(x), \qquad (D1)$$

where x_0, x_1 is determined by the normalization condition $1 = \langle 1 \rangle$, and the constraint on the first moment of J is $\langle J \rangle = \langle J - x_0 \rangle + x_0$. Using the relation

$$\langle (J - x_0)^n \rangle = 2A_\alpha D_L \langle J \rangle^\alpha \frac{x_1^{n-\alpha}}{\alpha - n} \qquad (D2)$$

we obtain

$$x_1 = \left(\frac{2A_\alpha D_L \langle J \rangle^\alpha}{\alpha} \right)^{1/\alpha}, \qquad (D3)$$

$$x_0 = \langle J \rangle - x_1 \frac{\alpha}{\alpha - 1}. \qquad (D4)$$

One can then sample values from this distribution using NumPy's `pareto` function.

For comparison with previous analyses [10,38], although the exact value of the common scale D_L depends on the shape of the synaptic strength distribution J_r, we have chosen it in computations to coincide, when $\alpha = 2$, with the diffusion approximation case where the synaptic strengths are constant for all neurons in each population. In this classical case, $|\langle J \rangle|^2 = \langle J^2 \rangle$, and so $D_L = 1/2$ using Eq. (A24).

[1] S. N. Dorogovtsev, A. V. Goltsev, and J. F. F. Mendes, Critical phenomena in complex networks, Rev. Mod. Phys. **80**, 1275 (2008).

[2] H. E. Stanley and P. Meakin, Multifractal phenomena in physics and chemistry, Nature (London) **335**, 405 (1988).

[3] M. A. Muñoz, Colloquium: Criticality and dynamical scaling in living systems, Rev. Mod. Phys. **90**, 031001 (2018).

[4] S. Ghashghaie, W. Breymann, J. Peinke, P. Talkner, and Y. Dodge, Turbulent cascades in foreign exchange markets, Nature (London) **381**, 767 (1996).

[5] W. Softky and C. Koch, The highly irregular firing of cortical cells is inconsistent with temporal integration of random EPSPs, J. Neurosci. **13**, 334 (1993).

[6] M. M. Churchland, B. M. Yu, J. P. Cunningham, L. P. Sugrue, M. R. Cohen, G. S. Corrado, W. T. Newsome, A. M. Clark, P. Hosseini, B. B. Scott *et al.*, Stimulus onset quenches neural variability: A widespread cortical phenomenon, Nat. Neurosci. **13**, 369 (2010).

[7] R. L. T. Goris, J. A. Movshon, and E. P. Simoncelli, Partitioning neuronal variability, Nat. Neurosci. **17**, 858 (2014).

[8] A. Renart, J. de la Rocha, P. Bartho, L. Hollender, N. Parga, A. Reyes, and K. D. Harris, The asynchronous state in cortical circuits, Science **327**, 587 (2010).

[9] C. van Vreeswijk and H. Sompolinsky, Chaos in neuronal networks with balanced excitatory and inhibitory activity, Science **274**, 1724 (1996).

[10] N. Brunel, Dynamics of sparsely connected networks of excitatory and inhibitory spiking neurons, J. Comput. Neurosci. **8**, 183 (2000).

[11] J. Kadmon and H. Sompolinsky, Transition to Chaos in Random Neuronal Networks, Phys. Rev. X **5**, 041030 (2015).

[12] A. Roxin, N. Brunel, D. Hansel, G. Mongillo, and C. van Vreeswijk, On the distribution of firing rates in networks of cortical neurons, J. Neurosci. **31**, 16217 (2011).

[13] M. Vegué and A. Roxin, Firing rate distributions in spiking networks with heterogeneous connectivity, Phys. Rev. E **100**, 022208 (2019).

[14] C. Schmeltzer, A. H. Kihara, I. M. Sokolov, and S. Rüdiger, Degree correlations optimize neuronal network sensitivity to sub-threshold stimuli, PLoS ONE **10**, e0121794 (2015).

[15] I. D. Landau, R. Egger, V. J. Dercksen, M. Oberlaender, and H. Sompolinsky, The impact of structural heterogeneity on excitation-inhibition balance in cortical networks, Neuron **92**, 1106 (2016).

[16] R. Rosenbaum, M. A. Smith, A. Kohn, J. E. Rubin, and B. Doiron, The spatial structure of correlated neuronal variability, Nat. Neurosci. **20**, 107 (2016).

[17] R. Rosenbaum and B. Doiron, Balanced Networks of Spiking Neurons with Spatially Dependent Recurrent Connections, Phys. Rev. X **4**, 021039 (2014).

[18] Y. Gu, Y. Qi, and P. Gong, Rich-club connectivity, diverse population coupling, and dynamical activity patterns emerging from local cortical circuits, PLoS Comput. Biol. **15**, e1006902 (2019).

[19] M. J. E. Richardson, Firing-rate response of linear and nonlinear integrate-and-fire neurons to modulated current-based and conductance-based synaptic drive, Phys. Rev. E **76**, 021919 (2007).

[20] M. J. E. Richardson and W. Gerstner, Synaptic shot noise and conductance fluctuations affect the membrane voltage with equal significance, Neural Comput. **17**, 923 (2005).

[21] S. Song, P. J. Sjöström, M. Reigl, S. Nelson, and D. B. Chklovskii, Highly nonrandom features of synaptic connectivity in local cortical circuits, PLoS Biol. **3**, e68 (2005).

[22] L. Cossell, M. F. Iacaruso, D. R. Muir, R. Houlton, E. N. Sader, H. Ko, S. B. Hofer, and T. D. Mrsic-Flogel, Functional organization of excitatory synaptic strength in primary visual cortex, Nature (London) **518**, 399 (2015).

[23] G. Buzsáki and K. Mizuseki, The log-dynamic brain: How skewed distributions affect network operations, Nat. Rev. Neurosci. **15**, 264 (2014).

[24] M. C. Teich, C. Heneghan, S. B. Lowen, T. Ozaki, and E. Kaplan, Fractal character of the neural spike train in the visual system of the cat, J. Opt. Soc. Am. A **14**, 529 (1997).

[25] B. J. He, Scale-free brain activity: Past, present, and future, Trends Cognit. Sci. **18**, 480 (2014).

[26] B. Munn, N. Zeater, A. N. Pietersen, S. G. Solomon, S. K. Cheong, P. R. Martin, and P. Gong, Fractal spike dynamics and neuronal coupling in the primate visual system, J. Physiol. **598**, 1551 (2020).

[27] A. Y. Y. Tan, Y. Chen, B. Scholl, E. Seidemann, and N. J. Priebe, Sensory stimulation shifts visual cortex from synchronous to asynchronous states, Nature (London) **509**, 226 (2014).

[28] D. Jercog, A. Roxin, P. Barthó, A. Luczak, A. Compte, and J. de la Rocha, Up-down cortical dynamics reflect state transitions in a bistable network, eLife **6**, e22425 (2017).

[29] M. F. Shlesinger, B. J. West, and J. Klafter, Lévy Dynamics of Enhanced Diffusion: Application to Turbulence, Phys. Rev. Lett. **58**, 1100 (1987).

[30] R. N. Mantegna and H. E. Stanley, Scaling behavior in the dynamics of an economic index, Nature (London) **376**, 46 (1995).

[31] V. Zaburdaev, S. Denisov, and J. Klafter, Lévy walks, Rev. Mod. Phys. **87**, 483 (2015).

[32] J. Klafter and I. M. Sokolov, Anomalous diffusion spreads its wings, Phys. World **18**, 29 (2005).

[33] M. F. Shlesinger, G. M. Zaslavsky, and J. Klafter, Strange kinetics, Nature (London) **363**, 31 (1993).

[34] R. Metzler and J. Klafter, The random walk's guide to anomalous diffusion: A fractional dynamics approach, Phys. Rep. **339**, 1 (2000).

[35] A. V. Chechkin, R. Metzler, V. Y. Gonchar, J. Klafter, and L. V. Tanatarov, First passage and arrival time densities for Lévy flights and the failure of the method of images, J. Phys. A: Math. Gen. **36**, L537 (2003).

[36] R. Metzler, E. Barkai, and J. Klafter, Deriving fractional Fokker-Planck equations from a generalised master equation, Europhys. Lett. **46**, 431 (1999).

[37] R. Metzler and T. F. Nonnenmacher, Space- and time-fractional diffusion and wave equations, fractional Fokker–Planck equations, and physical motivation, Chem. Phys. **284**, 67 (2002).

[38] N. Brunel and V. Hakim, Fast global oscillations in networks of integrate-and-fire neurons with low firing rates, Neural Comput. **11**, 1621 (1999).

[39] K. J. Miller, L. B. Sorensen, J. G. Ojemann, and M. den Nijs, Power-law scaling in the brain surface electric potential, PLoS Comput. Biol. **5**, e1000609 (2009).

[40] D. J. Amit and N. Brunel, Model of global spontaneous activity and local structured activity during delay periods in the cerebral cortex, Cereb. Cortex **7**, 237 (1997).

[41] L. Kuśmierz, S. Ogawa, and T. Toyoizumi, Edge of Chaos and Avalanches in Neural Networks with Heavy-Tailed Synaptic Weight Distribution, Phys. Rev. Lett. **125**, 028101 (2020).

[42] C.-T. Shih, Y.-J. Lin, C.-T. Wang, T.-Y. Wang, C.-C. Chen, T.-S. Su, C.-C. Lo, and A.-S. Chiang, Diverse community structures in the neuronal-level connectome of the *Drosophila* brain, Neuroinformatics **18**, 267 (2020).

[43] L. K. Scheffer, C. S. Xu, M. Januszewski, Z. Lu, S.-Y. Takemura, K. J. Hayworth, G. B. Huang, K. Shinomiya, J. Maitlin-Shepard, S. Berg *et al.*, A connectome and analysis of the adult *Drosophila* central brain, eLife **9**, e57443 (2020).

[44] V. V. Uchaikin and V. M. Zolotarev, *Chance and Stability: Stable Distributions and Their Applications* (VSP, Moscow, Russia, 1999).

[45] D. Schertzer, M. Larchevêque, J. Duan, V. V. Yanovsky, and S. Lovejoy, Fractional Fokker–Planck equation for nonlinear stochastic differential equations driven by non-Gaussian Lévy stable noises, J. Math. Phys. **42**, 200 (2001).

[46] T. Koren, M. A. Lomholt, A. V. Chechkin, J. Klafter, and R. Metzler, Leapover Lengths and First Passage Time Statistics for Lévy Flights, Phys. Rev. Lett. **99**, 160602 (2007).

[47] A. Wardak, First passage leapovers of Lévy flights and the proper formulation of absorbing boundary conditions, J. Phys. A: Math. Theor. **53**, 375001 (2020).

[48] N. H. Bingham, Maxima of sums of random variables and suprema of stable processes, Z. Wahrscheinlichkeitstheorie Verw. Geb. **26**, 273 (1973).

[49] N. H. Bingham, Limit theorems in fluctuation theory, Adv. Appl. Probab. **5**, 554 (1973).

[50] J. Bertoin, *Levy Processes* (Cambridge University Press, Cambridge, 2012).

[51] M. R. Evans, S. N. Majumdar, and G. Schehr, Stochastic resetting and applications, J. Phys. A: Math. Theor. **53**, 193001 (2020).

[52] D. J. Amit and M. V. Tsodyks, Quantitative study of attractor neural network retrieving at low spike rates: I. Substrate—spikes, rates and neuronal gain, Netw. Comput. Neural Syst. **2**, 259 (1991).

[53] W. R. Inc., Mathematica, version 12.0 (2019).

[54] M.-O. Gewaltig and M. Diesmann, Nest (NEural Simulation Tool), Scholarpedia **2**, 1430 (2007).

[55] P. C. Petersen and R. W. Berg, Lognormal firing rate distribution reveals prominent fluctuation–driven regime in spinal motor networks, eLife **5**, e18805 (2016).

[56] A. Litwin-Kumar and B. Doiron, Slow dynamics and high variability in balanced cortical networks with clustered connections, Nat. Neurosci. **15**, 1498 (2012).

[57] S. Wieland, D. Bernardi, T. Schwalger, and B. Lindner, Slow fluctuations in recurrent networks of spiking neurons, Phys. Rev. E **92**, 040901(R) (2015).

[58] A. Mazzoni, S. Panzeri, N. K. Logothetis, and N. Brunel, Encoding of naturalistic stimuli by local field potential spectra in networks of excitatory and inhibitory neurons, PLoS Comput. Biol. **4**, e1000239 (2008).

[59] F. Barbieri, A. Mazzoni, N. K. Logothetis, S. Panzeri, and N. Brunel, Stimulus dependence of local field potential spectra: Experiment versus theory, J. Neurosci. **34**, 14589 (2014).

[60] G. La Nave, K. Limtragool, and P. W. Phillips, Colloquium: Fractional electromagnetism in quantum matter and high-energy physics, Rev. Mod. Phys. **91**, 021003 (2019).

[61] A. Das and A. Levina, Critical Neuronal Models with Relaxed Timescale Separation, Phys. Rev. X **9**, 021062 (2019).

[62] S. di Santo, P. Villegas, R. Burioni, and M. A. Muñoz, Landau–Ginzburg theory of cortex dynamics: Scale-free avalanches emerge at the edge of synchronization, Proc. Natl. Acad. Sci. USA **115**, E1356 (2018).

[63] M. N. Shadlen and W. T. Newsome, The variable discharge of cortical neurons: Implications for connectivity, computation, and information coding, J. Neurosci. **18**, 3870 (1998).

[64] T. Hromádka, A. M. Zador, and M. R. DeWeese, Up states are rare in awake auditory cortex, J. Neurophysiol. **109**, 1989 (2013).

[65] G. Deco and E. Hugues, Neural network mechanisms underlying stimulus driven variability reduction, PLoS Comput. Biol. **8**, e1002395 (2012).

[66] L. Mazzucato, A. Fontanini, and G. La Camera, Dynamics of multistable states during ongoing and evoked cortical activity, J. Neurosci. **35**, 8214 (2015).

[67] A. Keane and P. Gong, Propagating waves can explain irregular neural dynamics, J. Neurosci. **35**, 1591 (2015).

[68] M. di Volo and A. Destexhe, Optimal responsiveness and collective oscillations emerging from the heterogeneity of inhibitory neurons, arXiv:2005.05596 [q-bio.NC].

[69] I. M. S. J. Klafter, *First Steps in Random Walks: From Tools to Applications* (Oxford University Press, Oxford, 2011).

[70] D. J. Amit and N. Brunel, Dynamics of a recurrent network of spiking neurons before and following learning, Netw., Comput. Neural Syst. **8**, 373 (1997).

[71] S. Jespersen, R. Metzler, and H. C. Fogedby, Lévy flights in external force fields: Langevin and fractional Fokker-Planck equations and their solutions, Phys. Rev. E **59**, 2736 (1999).